

# Identification and Analysis of Young Star Cluster Candidates in M31<sup>1</sup>

Benjamin F. Williams

University of Washington

Astronomy Dept. Box 351580, Seattle, WA 98195-1580

ben@astro.washington.edu

Paul W. Hodge

University of Washington

Astronomy Dept. Box 351580, Seattle, WA 98195-1580

hodge@astro.washington.edu

## ABSTRACT

We present a method for finding clusters of young stars in M31 using broadband WFPC2 data from the HST data archive. Applying our identification method to 13 WFPC2 fields, covering an area of  $\sim 60$  arcmin<sup>2</sup>, has revealed 79 new candidate young star clusters in these portions of the M31 disk. Most of these clusters are small ( $\lesssim 5$  pc) young ( $\sim 10$ -200 Myr) star groups located within large OB associations. We have estimated the reddening values and the ages of each candidate individually by fitting isochrones to the stellar photometry. We provide a catalog of the candidates including rough approximations of their reddenings and ages. We also look for patterns of cluster formation with galactocentric distance, but our rough estimates are not precise enough to reveal any clear patterns.

*Subject headings:* galaxies: M31; spiral; stellar populations; star clusters; OB associations.

---

<sup>1</sup>Based on observations with the NASA/ESA Hubble Space Telescope obtained at the Space Telescope Science Institute, which is operated by the Association of Universities for Research in Astronomy, Inc., under NASA contract NAS5-26555.

## 1. Introduction

Observations of extragalactic young star clusters are essential for understanding how star formation affects galaxy evolution. The young stellar population is responsible for many of the characteristics which give spiral galaxies their current morphological classification. Although massive young stars constitute only a very small percentage of the stellar population of most spiral galaxies, they trace the most recent star formation, produce and disperse most of the heavy elements, and illuminate the spiral arms. Open clusters are the typical birthplaces of bright massive stars. Since these clusters contain the youngest stars in the galaxy, their identification and examination is crucial for learning how star formation has progressed within the galaxy, resulting in its current appearance. The most detailed information about these clusters comes from studies of their constituent stars.

The study of extragalactic OB associations has been an ongoing struggle for 5 decades, going back to studies of the properties of the very conspicuous associations of bright stars in the Large Magellanic Cloud (LMC) in the 1950s (e.g. Buscombe, Gascoigne, & de Vaucouleurs 1955, Shapley 1956). Decades of research have resulted in catalogs of OB associations in nearby galaxies (e.g. Lucke & Hodge 1970 (LMC), van den Bergh 1964 (M31), Hodge 1977 (NGC 6822)). These catalogs have provided excellent starting points for studying the young stellar populations of other galaxies; however, these samples were not ideal for further statistical analysis because they were obtained through subjective analysis of low-resolution, non-uniform data.

More recently, high-resolution photometric data and advances in computational analysis techniques have allowed more objective identification of OB associations in galaxies (e.g. Wilson, Scoville, & Rice (1991)), creating more uniform samples on which to perform statistical analyses. These objective samples have resulted in significant advances in our understanding of the properties of extragalactic OB associations. The similarity of their size distributions and stellar luminosity functions across different galaxy types (Bresolin et al. 1998), and their similar luminosity function across galaxy types (Battinelli et al. 2000) have suggested that massive star formation occurs by similar processes in all galaxies. At the same time, OB associations’ average population sizes appear to differ between galaxies of different morphological type (Bresolin & Kennicutt 1997), showing that environment has some effect on massive star formation.

M31 has been an excellent laboratory for the study of massive star formation due to its proximity and its many active spiral arms. These arms contain hundreds of OB associations that have been studied extensively from the ground and from space. Our distant view of M31 has allowed ground-based studies of young clusters on a wide range of size scales. Due to the crowding of stars and variable reddening in the disk, the optical ground based

data was used mainly for identification and studies of the structure of OB associations. These studies have shown, for example, that massive star formation appears hierarchical (Battinelli, Efremov, & Magnier 1996): the large complexes contain many smaller clusters, possibly with related physical properties. In the infrared, the crowding and reddening effects are reduced. Recent infrared work has succeeded in finding evidence for episodic star formation which occurred in different subregions during each spiral wave passage (Kodaira et al. 1999). Space-based observations are allowing more detailed analysis of these regions of recent star formation. Magnier et al. (1997) have used Hubble Space Telescope (HST) photometric data to determine the reddening distribution and ages of a handful of OB associations.

While studies of the well-known OB associations in M31 have been instrumental to our understanding of massive star formation, there has been very little work done on the small, young and compact star clusters in the spiral arms of M31. These clusters have been difficult to identify from the ground since they require very high resolution to resolve. Hodge (1979) discovered several hundred open cluster candidates in M31, but these objects were larger than typical Galactic clusters and may actually be small OB associations. In this study, we use the resolving power of HST in order to probe the size scales of typical open clusters in M31. We create a cluster finding algorithm fine-tuned to find small young clusters in the M31 disk and identify their most likely member stars. We then use the photometry from these stellar populations to estimate reddening and age values for our sample of young cluster candidates.

## 2. Data Acquisition and Reduction

We searched the HST archive for all exposures of longer than 60 seconds which were taken through the broadband B (F439W) and V (F555W) filters pointing within 1.5 degrees of the M31 nucleus. Using this narrow radius kept our data contained within the disk, avoiding significant halo contamination. Any fields in the bulge were later excluded by eye. We acquired and reduced 13 WFPC2 fields from the HST archive, each observed through at least the B and V broad-band filters. U band (F336W) images were also available for most of these fields, providing useful information about the reddening of our cluster candidates. Table 1 gives the RA, DEC, dates, bandpasses, and exposure times of the data taken from the HST archive in order to put together each of these fields. The positions of these fields on the galaxy are shown in Figure 1. The figure shows an  $H\alpha$  mosaic of the M31 disk (Winkler & Williams 1995) with the positions of the 13 fields marked with squares showing the positions of each chip in the field. Each field is labeled with the number given in Table

1. The PC chip position is not shown because it was excluded from our analysis. Since the PC portions of the images often contained special regions of the galaxy (e.g. globular clusters) and since the area covered by the PC is small, we decided to exclude all of the PC data in order to keep the data set as unbiased as possible. The exposure times for these fields were generally quite short, and therefore they are relatively shallow.

We determined instrumental magnitudes for each of these fields using the automated programs DAOPHOT II and ALLSTAR (Stetson, Davis, & Crabtree 1990). An object was considered a real star if it was detected as a point source at  $4\sigma$  above the noise level in 2 bandpasses with centroids separated by less than 0.7 pixels. Therefore, some of the objects under consideration may be misclassified background galaxies and foreground stars; however, in fields of these angular sizes at this galactic latitude ( $-21.57^\circ$ ) and these depths, the average number of foreground galactic stars per field should be less than 10. Background galaxies will typically not be detected as they will not appear as point sources. Figures 2 and 3 show the typical photometric errors, determined by ALLSTAR, as a function of B and V magnitude for each of the 13 fields. The errors tended to be approximately at the 10% level near the bright magnitudes ( $m_V < 24$ ), mostly due to the fluctuating surface brightness of the background. The M31 disk is a complex background with which to work and therefore limits the accuracy of the photometry by increasing the uncertainty of the local background level. This uncertainty is partially due to the poisson noise of the higher background levels, but it is also due to actual structure in the background on spatial scales relevant to stellar photometry. These surface brightness fluctuations come from structure in the stellar disk which cannot be resolved by HST.

Point Spread Function (PSF) magnitudes were checked against aperture photometry of the most isolated stars with the highest signal to noise in order to determine if there was an offset between the PSF photometry and the more standard aperture photometry. We found small offsets of our PSF photometry from the aperture photometry on the WF3 chip in the V band and in the WF4 chip in the B band. We applied small corrections (+0.03 mags for stars measured in the V band on the WF3 chip, and +0.05 mags for stars measured in the B-band on the WF4 chip) to our photometry in these cases in order to make the mean offset between the aperture and PSF photometry zero. In all other cases, the offsets were zero. We then obtained standard U, B, and V magnitudes from our instrumental magnitudes using the methods, zero points, and transformation coefficients given in Holtzman et al. (1995). We first determined instrumental magnitudes for the F336W, F439W, and F555W filter as

$$m_{filter} = -2.5 \times \log(ADU/t) + X + ZP_{filter} \quad (1)$$

where ADU is the number of counts, t is the exposure time, X is the small offset computed from the aperture photometry mentioned above, and  $ZP_{filter}$  is the zero point of the

WFPC-2 chip for the bandpass. Since the transformation to U, B, and V is a function of color, we used the F336W - F439W as a first approximation of the U-B color and the F439W - F555W color as a first approximation of the B-V color and iteratively solved the transformation equations.

As a further test to the accuracy of our photometry, we took advantage of the fact that two of our fields were overlapping. The WF3 chip in field 7 was covering the same region of space as the WF2 chip in field 9. We used the IRAF<sup>2</sup> tasks GEOMAP and GEOTRAN to determine a rotational and translational conversion between the coordinates of the stars in one frame to their coordinates in the other frame. We were then able to convert all of the pixel coordinates of the stars in one frame to the coordinates of the same star in the other frame. By comparing the star lists, we found every star which was detected in both frames. Then we were able to compare independent measurements of the same stars as determined in different locations on the chips, on different chips and in different frames.

The easiest way to see the accuracy of our photometry is by looking at the residuals after subtracting the magnitudes of the stars determined on the WF3 chip from the same stars observed with the WF2 chip. These residuals are shown in Figure 4. No systematic differences between the chips are seen, and the residuals are consistent with zero in nearly all cases. With this reinforcement that we understood our errors, and with the knowledge that our photometry and errors were accurate, we could apply our young cluster finding algorithm to the stellar photometry.

### 3. Identification of Young Clusters of Stars

In order to explore the many open clusters and young stellar associations, we created an objective method for detecting the clusters within the fields. Using our stellar positions and photometry from DAOPHOT II and ALLSTAR, the mean surface density of bright ( $m_V < 24.5$ ,  $M_V \lesssim 0.1$ ) blue ( $B - V < 0.45$ ) stars is determined. Then the standard deviation from the mean density ( $\sigma$ ) on a size scale specified by the user is calculated. This calculation is performed by comparing the density of bright blue stars in regions of the specified size around every bright blue star detected in the field with the mean density. This calculation of the mean stellar density and the standard deviation of the stellar density is followed by a search for regions containing at least 4 bright blue stars and having surface

---

<sup>2</sup>IRAF is distributed by the National Optical Astronomy Observatories, which are operated by the Association of Universities for Research in Astronomy, Inc., under cooperative agreement with the National Science Foundation.

densities of bright blue stars  $3\sigma$  above the mean.

We found the user specified size must be chosen carefully. Large values will often find overdensities which contain more than one cluster, unnecessarily reducing the spatial resolution of the data. Small values will often lead to single clusters being divided into several stellar overdensities of the size requested. We found the best way to overcome these problems was to run the algorithm using two size scales, one corresponding to the sizes of a few of the smaller clusters visible in the images and one corresponding to the sizes a few of the larger clusters visible in the images. If a cluster was found at both size scales, we had to choose which of the detections was most appropriate to use for follow-up work. If the cluster appeared small and populous we would use the detection from the small search radius in order to avoid field contamination in our star sample. If the cluster was large, and it had been detected as more than one cluster with the small search radius, we would use the detection from the large search radius in order to maximize the number of stars in our sample and in order to avoid making multiple age and reddening measurements for the same cluster.

Finally, in order to remove statistical anomalies from our sample, we ran each cluster candidate through a surface brightness test. In this test, we measure the surface brightness around the center of each cluster candidate. This test was a bit more complex since, due to completeness issues, the centers of the stellar overdensities were not always aligned exactly with the high surface brightness regions. Therefore we allowed overdensities with very nearby high surface brightness regions to pass. This step required great care for the larger clusters since the chance of one bright star entering the surface brightness calculation and enhancing the surface brightness near the center of the overdensity was higher for the large clusters. We found the number of these single bright star contaminants was reduced when we removed candidates with substantial ( $>2$  mag arcsec $^{-2}$ ) increases in surface brightness away from the center. These large jumps in surface brightness were usually bright single point sources, which were likely foreground stars. Any stellar overdensity whose measured surface brightness characteristics did not pass our objective criteria was not likely part of an underlying cluster of unresolved stars. These low surface brightness regions were removed from the sample.

We ran this algorithm on our star lists for all of the WFPC2 chips for each field in our sample. We did one run looking for small scale associations (radius  $\sim 5$  pc), and we did a second run looking for larger associations (radius  $\sim 15$  pc). We compared our results with published catalogs of clusters and associations, and with previously performed eye searches in order to learn our method’s strengths and weaknesses. The only previously known blue cluster in the survey region was G42 (Sargent et al. 1977), and it was found

by our algorithm. Since these regions had not been observed for young clusters with this resolution before, all of the other coincident cataloged objects were either individual bright stars within the clusters or coincident emission nebulae within the confused northeast spiral arm. No other previously known star clusters were found. There were, however, a few distinct clusters found within objects which had been previously cataloged from the ground as a single cluster. For example, the previously cataloged H81 B-202 (Hodge 1981), which was an open cluster as seen from the ground contains three of these cluster candidates at high resolution: M31SCC J004205+405714, M31SCC J004204+405826, and M31SCC J004205+405659. This discovery may indicate that many open clusters found with ground based data could in fact be small OB associations containing multiple young clusters. The other clusters which were found to be part of previously cataloged clusters are listed in Table 3.

Due to the size of the fields we were using, we were not able to find large ( $>40$  pc) OB associations previously discovered from the ground, but we were able to identify smaller sub-clusters within these larger associations which were not previously identified as separate clusters. This selection bias against large associations should be avoidable in other data sets by looking for stellar overdensities on larger scales, but we did not have wide enough fields to run such a test. We also found that our method did not detect the smallest, densest clusters seen by eye, most likely due to the low completeness in these areas. It also missed several obvious red clusters, including a few known globulars. These clusters were either heavily extincted or much older than the clusters found by our algorithm. In either case, due to severe crowding, age, or extinction, there were too few detected blue stars in these clusters to separate the cluster stars from the field in order to study the stellar population.

Succinctly, the algorithm tended to miss many possible clusters that could be seen by eye. These clusters tended to be dense red clusters which were likely older than our sample and/or heavily reddened. Using different color criteria, it could be possible to obtain a sample of red cluster candidates; however, we limit our discussion here to the blue cluster candidates which were the most straight-forward to statistically separate from the background population. The clusters the algorithm did not find were too red or too dense to easily obtain photometry of a sample of member stars. The member stars did not stand out statistically in color, or due to completeness, they did not stand out in stellar density. The algorithm found only one previously known blue cluster in the images as well as many new clusters which were found previously by eye. Five of the fields had been previously scrutinized by eye looking for extended objects which may be clusters. Table 3 lists which of the star clusters found by the algorithm in these five fields were also found by eye, and which were not. Roughly 75 percent of the objects found by the algorithm had been previously discovered by eye on the test fields. The other 25 percent were comparable

to M31SCC J004455+413127 or M31SCC J004206+405649 (see Figure 5). They did not contain obvious compact cores and are not as likely to be real clusters.

We also checked the overlapping fields to see which clusters were found independently by the algorithm using photometry from different observations of the same region. Table 4 lists the clusters which were in the overlapping regions of two fields, along with the fields in which they were found. There were clusters found in overlapping regions of fields 9 and 10. Only 3 of 7 cluster candidates in the overlapping regions were found independently in both frames. This result reveals the dependence of our method upon the stellar density of the field observed. The non-overlapping regions of the overlapping fields sample different regions, and if these non-overlapping regions of the fields have significantly different mean stellar densities or significantly different stellar density fluctuations, then the algorithm will pick out some different cluster candidates for the overlapping regions of the fields. For example, the WF2 chip of field 10 overlaps the WF4 chip of field 9. The non-overlapping portion of the WF2 chip of field 10 contains a very active region. This active region raises the stellar density threshold for finding a cluster on the field 10 chip. Therefore the clusters found on the field 9 chip are not as convincing due to the very low average stellar density, and, in fact, these clusters are not picked out on the field 10 chip, even though field 10 is deeper. Exactly the inverse situation occurs for the non-overlapping portions of the WF3 chip of fields 9 and 10. Here the non-overlapping section of field 9 contains a very active region, raising the threshold for finding a cluster. This inconsistency would likely be less severe for wider field data sets, as the mean stellar densities and density fluctuations should be more stable if sampled over larger regions. The good news about these inconsistencies between overlapping regions is that they provide a very nice ranking of candidates in these regions. The candidates that were found in both data sets of the same area are much stronger than the candidates that were not.

We show a random subset of 9 of the objects detected by the algorithm in Figure 5. These 9 images are through the F439W filter and are 12 arcsec across. The example set shows a variety of objects from large obvious clusters like M31SCC J004000+403325 to very marginal detections such as M31SCC J004455+413127. There were several of these types of objects in our sample, which do not look like obvious clusters to the eye. These make up close to half of the sample. Generally, the properties of these cluster candidates are right at the limits of our criteria. The candidates that were not found independently when observed in two fields were comparable to these candidates, as were the candidates that were not seen by eye. Nevertheless these star populations contain well above the mean density of bright blue stars and have enhanced surface brightness compared to the rest of the region sampled in that field. There was no simple objective way to remove these objects from the sample without also removing many of our best candidates in the process. Though these



objects are less likely bona fide clusters, we have included them for completeness.

## 4. Determining Physical Parameters for the Clusters

### 4.1. Deprojected Galactocentric Distance

Using the coordinates of the clusters in the HST fields, RA=00:42:44.31 DEC=41:16:09.4 for the center of M31, the inclination angle of the disk (77 degrees) (Brinks & Burton 1984), and the position angle of the disk (38 degrees), we corrected the projected galactocentric distances of each of our fields. First we determined the major and minor axis coordinates using:

$$\begin{aligned} x^2 &= P^2 * \cos^2(\phi - \theta) \\ y^2 &= (P^2 - x^2) \end{aligned}$$

where  $x$  is the coordinate of the object along the major axis of M31,  $y$  is the coordinate of the object along the minor axis,  $\phi$  is the angular position of the object east of north,  $\theta$  is the M31 position angle east of north, and  $P$  is the projected galactocentric distance of the field. Then, we corrected the minor axis coordinate for the disk inclination using:

$$y_c^2 = y^2 / \cos^2(I)$$

where  $y_c$  is the minor axis coordinate corrected to its face-on value. Together, these transformations allow a direct transformation from  $P$  to the galactocentric distance using:

$$G^2 = x^2 + y_c^2 = P^2(\cos^2(\phi - \theta) + (1 - \cos^2(\phi - \theta))/\cos^2(I))$$

where  $G$  is the deprojected galactocentric distances for the clusters. Calculated values are given in Table 2.

### 4.2. Reddening and Age Determinations

Once we had determined the positions of the clusters and the photometry of the most likely member stars, the next step was to correct the stellar photometry for the extinction between us and each of the clusters. The reddening was likely to be significant since these

clusters were all within the M31 disk where we expect there to be relatively thick dust. Open clusters tend to contain upper main sequence stars. These stars are virtually the same intrinsic color in B-V, and they tend to lie along a narrow sequence in the U-B, B-V plane. Since extinction makes these stars appear to be to the red of this sequence, it is possible to estimate the extinction values of these clusters using photometry of just a few of the brightest cluster members.

Since the clusters were found on the basis of the grouping of just a handful of detected bright blue stars, we were limited in our confidence for determining accurate reddening and age values for them. Since there was not a statistical overdensity of red stars in the clusters, we could not confidently assume the red stars were cluster members. Therefore we had very few stars from each cluster with which to work, and it was not practical or informative to run a detailed fit of synthetic color-magnitude diagrams to the observed color-magnitude diagram. With so few stars, it proved more useful and faster to assume that the over-dense population of blue stars we detected represented the main sequence turnoff of the cluster. Simulations described in section 4.3 show this to be a reasonable assumption to estimate the age to  $\sim 50\%$  accuracy. This assumption allowed us to determine reddening values by fitting model U-B and B-V star colors to model main sequence colors when possible. We determined the reddening by doing a least-squares fit of the U-B and B-V colors of the stars to the U-B and B-V colors of the theoretical main sequence from Girardi et al. (2000). We occasionally adjusted this value in cases where the B-V colors of the full cluster sample did not appear to follow the isochrones due to one outlier which had polluted the least-squares fit. In cases where there were no U band data available, the reddening was determined by fitting the B-V colors to the theoretical upper main sequence. The reddening values for the whole sample determined by this method are given in Table 2.

Figure 6 shows a sample of one of our reddening determination fits. The figure shows the data after applying the our best reddening correction overplotted with the theoretical stellar colors from Girardi et al. (2000). In some cases, only one star was detected in all three bands due to the sensitivity of WFPC2 in the UV. These single star fits often had to be adjusted by eye since they often resulted in poor fits to the B-V color for the rest of the stars detected in the cluster candidate. These adjustments pushed the stars slightly off the best fit to the theoretical line in these cases. Our findings show that these clusters have a wide range of reddening values, indicating that they are likely at different depths within the disk. In the cases where U band data was not available, the reddening had to be fit assuming that all of the stars were still on the upper main sequence, and therefore were not red in B-V due to evolution. Two examples of these fits are shown in Figure 6 as well. We assume that all of the stars within a single cluster are reddened by the same amount. It is possible that some of these clusters contain dust which would produce differential

reddening within individual clusters. If differential reddening is affecting our data, it is possible that the brightest stars are over-corrected. Such an over correction would cause an under-estimation of the cluster age as determined by the method described below.

After correcting the photometry using these reddening values, we produced simple least-squares fits of the stellar photometry to single age model isochrones in order to approximate the age of the cluster. This procedure was performed on all of our cluster candidates. We used all of the stars in the overdensity, without subtracting any possible field stars. We justify the lack of correcting for field contamination by pointing out that the average number of these bright blue stars in areas the size that we were sampling was generally  $\lesssim 1$ . Randomly throwing out a single star from each cluster would not have been useful in case of our data because there was no reason to throw out one star as opposed to another. On the contrary, these stars had already been selected on the basis that they were grouped, bright blue stars of which the density in the field was very low. Therefore, our field contamination was minimized without doing a second contamination correction. All of the age fits were inspected by eye and adjusted in cases where the fitting procedure produced inferior fits. The inferior fits were obvious because they did not fit the main sequence turnoff of the cluster due to the measured color of the brightest star in the cluster. If this color was measured to be bluer than the theoretical main sequence due to photometry errors, then the least squares method could not fit a turnoff. In these cases, ages were determined using by-eye fits to the isochrones. Therefore, about half of our age determinations were done by eye, and the fitting procedure was only used as a first approximation. Some typical fits are shown in Figure 7. The ages for the whole sample determined by this method are given in Table 2.

### 4.3. Error Estimates: Simulation Tests

We determined the errors of our subjective age and reddening determination technique through several experiments. First, we simulated our data using higher resolution PC data of well-studied massive young clusters. By comparing the results from our crude method to the robust results from the high resolution data, we were able to estimate how accurate our results were for the most populated clusters. Then we experimented with the clusters themselves. By removing data points and iterating our analysis routine, we were able to assess the stability of our results. Lower stability resulted in errors larger than those determined by the resolution simulation.

As a test of our age and reddening determination method, we simulated our low resolution wide field data using our data from the PC. Since we had previously obtained

robust ages from the high resolution PC data of four previously known blue globular-like clusters (Williams & Hodge 2001), we binned these data 2 by 2 in order to simulate the resolution of the WF chips ( $\sim 0.1$  arcsec/pixel). We then ran the binned data through the same photometry routine and cluster finding algorithm as the wide field data. This exercise was further confirmation that the algorithm was finding clusters, as it found all four clusters and nothing else in the frames. Finally, we put the stars which the algorithm provided as the most likely cluster members through the same reddening and age determination routine in order to check the accuracy of our method. We found that the ages determined were all under-estimated. The turn-off was found at a brighter magnitude than we had determined it from the PC. These brighter turnoff stars were always found very near the cluster center, and therefore were very likely blended stars at the lower resolution. These massive and dense clusters show the worst case scenario for this kind of blending, so that we hope our less populous clusters will not suffer as badly from this effect.

A summary of the results of the low resolution simulation is shown in Table 5. The ages are systematically under estimated by a mean of 0.2 dex. Since the vast majority of the new cluster candidates were not this dense and massive, we did not feel that it would be appropriate to simply add 0.2 dex to all of our ages. Rather, this result was useful for determining our error bars. The test showed that  $\pm 0.2$  dex was the best we could do for our age determinations. The test result also showed that error determination by throwing out the brightest few stars at the turnoff and redetermining the reddening and age was reasonable.

In order to assess the errors of our reddening and age estimates for each cluster candidate individually, we removed the brightest star from each small cluster and the brightest four stars from every large cluster. We then measured the reddening and age again using the same method. This experiment allowed us to find the stability of our estimate as well as to account for the effect of field stars, and/or blends on our results. The errors given are the difference between the reddening and age values determined with the full sample of stars and the values determined with the manipulated sample. If this error value was less than 0.1 in  $E_{B-V}$  or 0.2 in log age, the error was set to 0.1 in  $E_{B-V}$  or 0.2 in log age because our low resolution simulation had shown that our errors had to be at least this large. We therefore would not allow these reddening and age values, determined using a much smaller number of stars, to have smaller quoted errors. These small experimental errors were quite common, mostly due to the high sensitivity of the turnoff to the age at these young ages (2 mag between 30 Myr and 100 Myr). It was encouraging to find that most of our experiments showed our results to be quite stable against removal of the turnoff data points.

## 5. Results and Conclusions

All of our measurements are given in Table 2. With this table, we have provided an objective collection of young star cluster candidates in the M31 disk along with their reddenings and ages as determined from the photometry of their constituent stars. With our crude age approximations, it was possible to look for statistical patterns in the age distribution. While the precision of our ages is clearly low, and in fact we cannot even quote reliable errors on our age measurements, our data is most sensitive to bright blue stars which define the main sequence turnoff of these clusters. Assuming the detected stars do mark the turnoff, and that our data set was equally sensitive to them for all of the clusters detected, we believe that we have done the best job possible to preserve their relative ages by reducing all of the data identically and determining all ages with the same model isochrones.

We looked for correlations between the reddening of the clusters and their galactocentric distances and between the ages of the clusters and their galactocentric distances. These plots are shown in Figure 8. No correlation is seen within the large errors in our measurements. Apparently, more accurate age determinations are needed in order to decipher the propagation of recent cluster formation in these regions of the M31 disk. We also checked for a correlation between ages and reddening which would have been indicative of observational biases within the sample. As seen in Figure 9, there appears to be a lack of older clusters with high reddening values, confirming that our selection method is bias against such clusters. There is also a lack of older clusters with very low reddening. This effect was not expected, and it may be an effect of field contaminants. It is possible that the six clusters with very low reddening have field contaminants causing them to appear less reddened and younger.

We have created an automated routine for finding young star clusters among stellar populations in nearby galaxies. This method requires the clusters to be resolved into individual stars, so that the positions and photometric properties of the stars can be used to distinguish the star cluster candidate from the field. From comparisons between overlapping data sets and comparisons between the automated routine and independent searches by eye, we expect at least half of these candidates are real, young star clusters. The method is not effective for finding small compact clusters whose stellar populations cannot be studied in detail with the survey data. Unfortunately, the algorithm misses clusters that could be useful when higher resolution data are obtainable, and the algorithm finds some very loose associations which are likely not real clusters. On the other hand, the method is quite effective at finding star clusters whose populations can be further studied with the survey data. The algorithm only finds clusters whose stellar photometry is statistically different

from the surrounding stellar population. This statistical difference provides a sample of stars from each cluster candidate which can be used to constrain the age and reddening.

We have objectively detected 80 blue cluster candidates in the M31 disk using HST/WFPC2 archival data of 13 fields. Of these clusters, 79 are newly discovered as individual clusters, though many lie within previously known OB associations. We have determined rough ages and extinction estimates from the stellar photometry. The ages and reddening values for these clusters span the full range of our sensitivity and are consistent with the range of ages and reddening values of the OB associations determined by Magnier et al. (1997) in the fields common to both studies. The precision of our approximations is too low to look for cluster formation patterns; however, future, more accurate determinations of these values could significantly advance our understanding of the propagation of cluster formation in the M31 disk.

## 6. Acknowledgments

Support for this work was provided by NASA through grant number GO-06459.01-95A from the Space Telescope Science Institute, which is operated by the Association of Universities for Research in Astronomy, Incorporated, under NASA contract NAS5-26555.

## REFERENCES

- Battinelli, P., Capuzzo-Dolcetta, R., Hodge, P. W., Vicari, A., & Wyder, T. K. 2000, *A&A*, 357, 437
- Battinelli, P., Efremov, Y., & Magnier, E. A. 1996, *A&A*, 314, 51
- Bresolin, F., & Kennicutt, R. C. 1997, *AJ*, 113, 975
- Bresolin, F., et al. 1998, *AJ*, 116, 119
- Brinks, E., & Burton, W. B. 1984, *A&A*, 141, 195
- Buscombe, W., Gascoigne, S. C. B., & de Vaucouleurs, G. 1955, *Suppl. Australian J. Sci.*, 17
- Girardi, L., Bressan, A., Bertelli, G., & Chiosi, C. 2000, *A&AS*, 141, 371
- Hodge, P. W. 1977, *ApJS*, 33, 69

- Hodge, P. W. 1979, *AJ*, 84, 744
- Hodge, P. W. 1981, *Atlas of the Andromeda galaxy* (Seattle/London: University of Washington Press, 1981)
- Holtzman, J. A., Burrows, C. J., Casertano, S., Hester, J. J., Trauger, J. T., Watson, A. M., & Worthey, G. 1995, *PASP*, 107, 1065
- Kodaira, K., Vansevicius, V., Tamura, M., & Miyazaki, S. 1999, *ApJ*, 519, 153
- Lucke, P. B., & Hodge, P. W. 1970, *AJ*, 75, 171
- Magnier, E. A., Hodge, P., Battinelli, P., Lewin, W. H. G., & van Paradijs, J. 1997, *MNRAS*, 292, 490
- Sargent, W. L. W., Kowal, C. T., Hartwick, F. D. A., & van den Bergh, S. 1977, *AJ*, 82, 947
- Shapley, H. 1956, *Am. Sci.*, 44, 73
- Stetson, P. B., Davis, L. E., & Crabtree, D. R. 1990, in *ASP Conf. Ser. 8: CCDs in astronomy*, 289
- van den Bergh, S. 1964, *ApJS*, 9, 65
- Williams, B. F., & Hodge, P. W. 2001, *ApJ*, 548, 190
- Wilson, C. D., Scoville, N., & Rice, W. 1991, *AJ*, 101, 1293
- Winkler, P. F., & Williams, B. F. 1995, in *American Astronomical Society Meeting*, Vol. 186, 4910

Table 1. Data obtained from the HST data archive used for the cluster survey.

Field	Prop. #	Obs. date	RA (2000)	DEC (2000)	Filter	Exp. (sec)
1	8296	Oct 15 1999	0:39:47.35	40:31:57.9	F336W	1000
1	8296	Oct 15 1999	0:39:47.35	40:31:57.9	F336W	800
1	8296	Oct 15 1999	0:39:47.35	40:31:57.9	F336W	1200
1	8296	Oct 15 1999	0:39:47.35	40:31:57.9	F336W	600
1	8296	Oct 15 1999	0:39:47.35	40:31:57.9	F439W	800
1	8296	Oct 15 1999	0:39:47.35	40:31:57.9	F439W	800
1	8296	Oct 15 1999	0:39:47.35	40:31:57.9	F555W	600
1	8296	Oct 15 1999	0:39:47.35	40:31:57.9	F555W	600
2	8296	Oct 30 1999	0:40:01.58	40:34:14.7	F336W	1000
2	8296	Oct 30 1999	0:40:01.58	40:34:14.7	F336W	800
2	8296	Oct 30 1999	0:40:01.58	40:34:14.7	F336W	1200
2	8296	Oct 30 1999	0:40:01.58	40:34:14.7	F336W	600
2	8296	Oct 30 1999	0:40:01.58	40:34:14.7	F439W	800
2	8296	Oct 30 1999	0:40:01.58	40:34:14.7	F439W	800
2	8296	Oct 30 1999	0:40:01.58	40:34:14.7	F555W	600
2	8296	Oct 30 1999	0:40:01.58	40:34:14.7	F555W	600
3	6038	Jan 23 1996	0:40:14.10	40:37:11.3	F336W	900
3	6038	Jan 23 1996	0:40:14.10	40:37:11.3	F336W	900
3	6038	Jan 23 1996	0:40:14.10	40:37:11.3	F439W	600
3	6038	Jan 23 1996	0:40:14.10	40:37:11.3	F555W	160
4	6431	Dec 9 1997	0:40:39.54	40:33:25.4	F439W	350
4	6431	Dec 9 1997	0:40:39.54	40:33:25.4	F439W	350
4	6431	Dec 9 1997	0:40:39.54	40:33:25.4	F555W	260
4	6431	Dec 9 1997	0:40:39.54	40:33:25.4	F555W	260
4	6431	Dec 9 1997	0:40:39.54	40:33:25.4	F814W	260
4	6431	Dec 9 1997	0:40:39.54	40:33:25.4	F814W	260
5	8296	Oct 30 1999	0:41:22.08	40:37:06.7	F336W	600
5	8296	Oct 30 1999	0:41:22.08	40:37:06.7	F336W	1000
5	8296	Oct 30 1999	0:41:22.08	40:37:06.7	F336W	800
5	8296	Oct 30 1999	0:41:22.08	40:37:06.7	F336W	1200
5	8296	Oct 30 1999	0:41:22.08	40:37:06.7	F439W	800
5	8296	Oct 30 1999	0:41:22.08	40:37:06.7	F439W	800
5	8296	Oct 30 1999	0:41:22.08	40:37:06.7	F555W	600
5	8296	Oct 30 1999	0:41:22.08	40:37:06.7	F555W	600



Table 1—Continued

Field	Prop. #	Obs. date	RA (2000)	DEC (2000)	Filter	Exp. (sec)
6	6431	Dec 9 1997	0:42:05.27	40:57:33.9	F439W	350
6	6431	Dec 9 1997	0:42:05.27	40:57:33.9	F439W	350
6	6431	Dec 9 1997	0:42:05.27	40:57:33.9	F555W	260
6	6431	Dec 9 1997	0:42:05.27	40:57:33.9	F555W	260
6	6431	Dec 9 1997	0:42:05.27	40:57:33.9	F814W	260
6	6431	Dec 9 1997	0:42:05.27	40:57:33.9	F814W	260
7	5911	Oct 3 1995	0:44:44.17	41:27:33.8	F336W	400
7	5911	Oct 3 1995	0:44:44.23	41:27:33.8	F439W	160
7	5911	Oct 3 1995	0:44:44.23	41:27:33.8	F555W	140
8	8296	Oct 31 1999	0:44:46.19	41:51:33.3	F336W	1000
8	8296	Oct 31 1999	0:44:46.19	41:51:33.3	F336W	800
8	8296	Oct 31 1999	0:44:46.19	41:51:33.3	F336W	1200
8	8296	Oct 31 1999	0:44:46.19	41:51:33.3	F336W	600
8	8296	Oct 31 1999	0:44:46.19	41:51:33.3	F439W	800
8	8296	Oct 31 1999	0:44:46.19	41:51:33.3	F439W	800
8	8296	Oct 31 1999	0:44:46.19	41:51:33.3	F555W	600
8	8296	Oct 31 1999	0:44:46.19	41:51:33.3	F555W	600
9	5911	Oct 8 1995	0:44:49.28	41:28:59.0	F336W	400
9	5911	Oct 8 1995	0:44:49.34	41:28:59.0	F439W	160
9	5911	Oct 8 1995	0:44:49.34	41:28:59.0	F555W	140
10	6038	Jan 1 1996	0:44:51.22	41:30:03.7	F336W	900
10	6038	Jan 1 1996	0:44:51.22	41:30:03.7	F336W	900
10	6038	Jan 1 1996	0:44:51.22	41:30:03.7	F439W	600
10	6038	Jan 1 1996	0:44:51.22	41:30:03.7	F555W	160
11	5911	Oct 4 1995	0:44:57.57	41:30:51.6	F336W	400
11	5911	Oct 4 1995	0:44:57.63	41:30:51.6	F439W	160
11	5911	Oct 4 1995	0:44:57.63	41:30:51.6	F555W	140
12	5911	Oct 15 1995	0:45:09.20	41:34:30.5	F336W	400
12	5911	Oct 15 1995	0:45:09.25	41:34:30.7	F439W	160
12	5911	Oct 15 1995	0:45:09.25	41:34:30.7	F555W	140
13	5911	Oct 15 1995	0:45:11.89	41:36:56.8	F336W	400
13	5911	Oct 15 1995	0:45:11.95	41:36:57.0	F439W	160
13	5911	Oct 15 1995	0:45:11.95	41:36:57.0	F555W	140

Table 2. Catalog of positions, galactocentric distances, age estimates, reddening values, and search radii for M31 young star cluster candidates.

ID <sup>a</sup>	RA (2000)	DEC (2000)	GCD (kpc)	log AGE	$E_{B-V}$	$R_s^b$ (pc)
M31SCC J003952+403141	0:39:52.43	40:31:41.27	15.21	8.00±0.20	0.28±0.10	5
M31SCC J004000+403325	0:40:00.03	40:33:25.02	14.52	7.90±0.35	0.22±0.10	15
M31SCC J004000+403406 (G42)	0:40:00.83	40:34:06.64	14.49	7.75±0.45	0.21±0.10	15
M31SCC J004001+403420	0:40:01.54	40:34:20.06	14.44	8.25±0.30	0.20±0.20	5
M31SCC J004004+403440	0:40:04.66	40:34:40.51	14.11	8.10±0.20	0.23±0.10	5
M31SCC J004006+403508	0:40:06.78	40:35:08.41	13.92	7.30±0.85	0.25±0.10	15
M31SCC J004010+403624	0:40:10.36	40:36:24.16	13.63	7.75±0.60	0.01±0.10	5
M31SCC J004012+403632	0:40:12.01	40:36:32.62	13.46	7.70±0.50	0.24±0.10	5
M31SCC J004012+403617	0:40:12.97	40:36:17.32	13.33	7.90±0.45	0.17±0.10	15
M31SCC J004013+403815	0:40:13.68	40:38:15.54	13.46	7.70±0.40	0.43±0.10	5
M31SCC J004015+403652	0:40:15.42	40:36:52.85	13.11	7.90±0.20	0.35±0.10	5
M31SCC J004032+403320	0:40:32.93	40:33:20.45	12.10	7.90±0.20	0.16±0.10	5
M31SCC J004033+403308a	0:40:33.28	40:33:08.64	12.13	7.75±0.20	0.31±0.10	5
M31SCC J004033+403326	0:40:33.46	40:33:26.93	12.06	7.85±0.20	0.30±0.10	5
M31SCC J004033+403319	0:40:33.48	40:33:19.15	12.09	7.75±0.40	0.30±0.10	5
M31SCC J004033+403308b	0:40:33.51	40:33:08.39	12.12	8.00±0.20	0.24±0.10	5
M31SCC J004033+403346	0:40:33.70	40:33:46.69	11.99	8.00±0.20	0.34±0.10	5
M31SCC J004034+403351	0:40:34.62	40:33:51.59	11.95	8.00±0.20	0.32±0.10	15
M31SCC J004035+403420	0:40:35.45	40:34:20.24	11.83	7.90±0.20	0.28±0.10	5
M31SCC J004035+403251	0:40:35.51	40:32:51.18	12.15	7.85±0.20	0.22±0.10	5
M31SCC J004039+403210	0:40:39.35	40:32:10.79	12.32	8.15±0.35	0.31±0.18	5
M31SCC J004040+403223	0:40:40.43	40:32:23.50	12.26	7.85±0.20	0.27±0.10	5

Table 2—Continued

ID <sup>a</sup>	RA (2000)	DEC (2000)	GCD (kpc)	log AGE	$E_{B-V}$	$R_s^b$ (pc)
M31SCC J004040+403256	0:40:40.67	40:32:56.98	12.10	8.10±0.40	0.37±0.10	5
M31SCC J004041+403222	0:40:41.35	40:32:22.88	12.27	7.90±0.30	0.22±0.10	5
M31SCC J004117+403720	0:41:17.21	40:37:20.57	11.92	7.85±0.20	0.34±0.11	5
M31SCC J004119+403748	0:41:19.57	40:37:48.79	11.89	8.10±0.40	0.27±0.13	5
M31SCC J004121+403638	0:41:21.37	40:36:38.84	12.65	7.45±0.40	0.45±0.10	5
M31SCC J004123+403726	0:41:23.89	40:37:26.98	12.47	7.85±0.70	0.02±0.10	5
M31SCC J004125+403723	0:41:25.92	40:37:23.66	12.71	8.20±0.45	0.29±0.28	5
M31SCC J004158+405738	0:41:58.57	40:57:38.48	5.40	7.80±0.30	0.50±0.10	5
M31SCC J004204+405826 (H81 B-202)	0:42:04.85	40:58:26.44	5.47	7.95±0.20	0.43±0.11	5
M31SCC J004205+405714 (H81 B-202)	0:42:05.59	40:57:14.26	6.15	7.30±0.20	0.22±0.10	5
M31SCC J004205+405659 (H81 B-202)	0:42:05.80	40:56:59.06	6.31	7.75±0.45	0.37±0.10	5
M31SCC J004206+405649	0:42:06.23	40:56:49.38	6.45	7.40±0.45	0.35±0.10	5
M31SCC J004207+405801	0:42:07.11	40:58:01.27	5.89	7.25±0.55	0.35±0.10	15
M31SCC J004441+412701	0:44:41.19	41:27:01.37	17.32	7.45±0.20	0.38±0.10	5
M31SCC J004441+415136	0:44:41.35	41:51:36.86	10.37	8.05±0.20	0.24±0.10	5
M31SCC J004441+415239	0:44:41.61	41:52:39.22	10.50	7.75±0.30	0.29±0.10	5
M31SCC J004441+415123	0:44:41.79	41:51:23.15	10.37	8.05±0.20	0.41±0.10	5
M31SCC J004442+415237	0:44:42.09	41:52:37.45	10.52	7.95±0.20	0.34±0.10	5
M31SCC J004442+415153	0:44:42.48	41:51:53.42	10.46	7.85±0.20	0.35±0.10	5
M31SCC J004444+412749	0:44:44.86	41:27:49.32	17.63	7.40±0.60	0.22±0.10	5
M31SCC J004445+412800	0:44:45.07	41:28: 0.48	17.58	7.95±0.20	0.41±0.14	5
M31SCC J004445+415121	0:44:45.39	41:51:21.42	10.61	7.75±0.20	0.35±0.10	5

Table 2—Continued

ID <sup>a</sup>	RA (2000)	DEC (2000)	GCD (kpc)	log AGE	$E_{B-V}$	$R_s^b$ (pc)
M31SCC J004445+415208	0:44:45.68	41:52:08.65	10.68	8.25±0.20	0.30±0.10	5
M31SCC J004445+415107	0:44:45.73	41:51:07.88	10.63	7.50±0.45	0.26±0.10	5
M31SCC J004447+415238	0:44:47.06	41:52:38.21	10.81	8.05±0.20	0.42±0.10	5
M31SCC J004447+412821	0:44:47.32	41:28:21.97	17.84	7.70±0.20	0.02±0.10	5
M31SCC J004447+412843	0:44:47.74	41:28:43.82	17.73	7.30±0.35	0.27±0.10	15
M31SCC J004448+412925	0:44:48.43	41:29:25.15	17.52	7.75±0.20	0.02±0.10	5
M31SCC J004449+413034	0:44:49.04	41:30:34.78	17.07	7.55±0.20	0.55±0.10	5
M31SCC J004449+412924	0:44:49.25	41:29:24.97	17.68	7.50±0.50	0.23±0.10	5
M31SCC J004449+415131	0:44:49.86	41:51:31.39	10.97	7.70±0.20	0.42±0.10	5
M31SCC J004450+415211	0:44:50.26	41:52:11.50	11.00	8.15±0.30	0.18±0.10	5
M31SCC J004450+412917	0:44:50.38	41:29:17.95	17.96	7.60±0.35	0.29±0.10	5
M31SCC J004450+412914	0:44:50.97	41:29:14.60	18.11	7.50±0.20	0.16±0.10	5
M31SCC J004451+412924	0:44:51.32	41:29:24.83	18.09	7.50±0.50	0.02±0.10	5
M31SCC J004451+412911	0:44:51.74	41:29:11.44	18.28	7.35±0.40	0.13±0.10	15
M31SCC J004452+415144	0:44:52.35	41:51:44.21	11.19	7.80±0.25	0.23±0.10	5
M31SCC J004453+412927	0:44:53.52	41:29:27.82	18.49	7.80±0.30	0.21±0.10	5
M31SCC J004455+413127	0:44:55.90	41:31:27.16	17.96	7.65±0.20	0.24±0.10	5
M31SCC J004456+413121	0:44:56.02	41:31:21.54	18.03	7.35±0.20	0.21±0.10	5
M31SCC J004457+413123	0:44:57.73	41:31:23.30	18.35	7.70±0.20	0.01±0.10	5
M31SCC J004458+413049	0:44:58.97	41:30:49.21	18.87	7.65±0.40	0.33±0.10	5
M31SCC J004500+413057	0:45:00.93	41:30:57.71	19.18	7.30±0.40	0.41±0.10	15
M31SCC J004503+413408	0:45:03.82	41:34:08.54	18.19	7.90±0.25	0.20±0.10	5

Table 2—Continued

ID <sup>a</sup>	RA (2000)	DEC (2000)	GCD (kpc)	log AGE	$E_{B-V}$	$R_s^b$ (pc)
M31SCC J004504+413451	0:45:04.52	41:34:51.60	17.99	7.95±0.20	0.25±0.30	5
M31SCC J004506+413406	0:45:06.32	41:34:06.96	18.68	7.70±0.20	0.45±0.10	5
M31SCC J004506+413545	0:45:06.73	41:35:45.78	17.99	8.00±0.50	0.21±0.20	15
M31SCC J004509+413643	0:45:09.82	41:36:43.31	18.14	7.80±0.20	0.10±0.10	5
M31SCC J004509+413649	0:45:09.82	41:36:49.79	18.09	7.30±0.50	0.31±0.10	5
M31SCC J004510+413645	0:45:10.33	41:36:45.47	18.22	7.25±0.20	0.14±0.10	5
M31SCC J004511+413711	0:45:11.82	41:37:11.86	18.30	7.90±0.30	0.24±0.10	5
M31SCC J004512+413715	0:45:12.31	41:37:15.78	18.36	7.95±0.20	0.11±0.10	5
M31SCC J004512+413716	0:45:12.48	41:37:16.82	18.38	7.70±0.40	0.33±0.10	5
M31SCC J004512+413723	0:45:12.78	41:37:23.45	18.39	8.00±0.50	0.23±0.10	5
M31SCC J004512+413727	0:45:12.87	41:37:27.80	18.38	7.80±0.20	0.25±0.10	5
M31SCC J004513+413735	0:45:13.40	41:37:35.08	18.42	7.30±0.20	0.46±0.10	5
M31SCC J004514+413743	0:45:14.13	41:37:43.72	18.49	7.35±0.20	0.39±0.10	5
M31SCC J004514+413724	0:45:14.22	41:37:24.31	18.66	7.70±0.20	0.36±0.10	5

<sup>a</sup>M31SCC is an IAU registered acronym; G42 refers to the globular cluster catalog of Sargent et al. (1977); [H81] B-202 is identified in Hodge (1981)

<sup>b</sup>Search radius given to the automated search routine. Using this radius the algorithm searched for overdensities over areas of ( $\pi R_s^2$ ).

Table 3. Comparison of 5 fields searched both by eye and by algorithm. About 75 percent of the cluster candidates were found by both methods. Many of the candidates are parts of previously known associations.

Field	Cluster	Found by eye?	Association <sup>a</sup>
7	M31SCC J004441+412701	N	
7	M31SCC J004444+412749	Y	
7	M31SCC J004445+412800	N	
7	M31SCC J004447+412821	Y	
9	M31SCC J004447+412843	Y	Part of [H81] B-298
9	M31SCC J004451+412911	Y	Part of [H81] B-301
9	M31SCC J004453+412927	N	
11	M31SCC J004455+413127	Y	Part of [H81] B-306
11	M31SCC J004456+413121	Y	Part of [H81] B-306
11	M31SCC J004457+413123	Y	
11	M31SCC J004458+413049	Y	
11	M31SCC J004500+413057	Y	
12	M31SCC J004503+413408	Y	
12	M31SCC J004504+413451	N	
12	M31SCC J004506+413406	N	
12	M31SCC J004506+413545	N	
13	M31SCC J004509+413643	Y	Part of [H81] B-310
13	M31SCC J004509+413649	Y	Part of [H81] B-310
13	M31SCC J004510+413645	Y	Part of [H81] B-310
13	M31SCC J004511+413711	Y	
13	M31SCC J004512+413715	Y	Part of [H81] B-312
13	M31SCC J004512+413716	Y	Part of [H81] B-312
13	M31SCC J004512+413723	N	Part of [H81] B-312
13	M31SCC J004512+413727	Y	
13	M31SCC J004513+413735	Y	
13	M31SCC J004514+413743	Y	
13	M31SCC J004514+413724	Y	

<sup>a</sup>M31SCC is an IAU registered acronym; the [H81] B prefix is identified in Hodge (1981) table B.

Table 4. Comparison of detection cluster candidates appearing in more than one field.

Cluster	Fields Observed	Fields Found
M31SCC J004448+412925	9,10	10
M31SCC J004449+412924	9,10	10
M31SCC J004450+412914	9,10	9,10
M31SCC J004450+412917	9,10	9,10
M31SCC J004451+412924	9,10	9,10
M31SCC J004451+412911	9,10	9
M31SCC J004453+412927	9,10	9

Table 5. Comparison of ages determined by isochrone fitting on high and low resolution WFPC2 photometry.

Name	$\log \text{Age}_{\text{ hires }} \text{ (yr)}$	$\log \text{Age}_{\text{ lowres }} \text{ (yr)}$	$E(B-V)_{\text{ hires }}$	$E(B-V)_{\text{ lowres }}$
G38	$8.00 \pm 0.15$	$7.75 \pm 0.20$	$0.31 \pm 0.11$	$0.26 \pm 0.10$
G44	$8.00 \pm 0.15$	$7.90 \pm 0.20$	$0.23 \pm 0.10$	$0.21 \pm 0.10$
G94	$8.20 \pm 0.15$	$7.80 \pm 0.20$	$0.20 \pm 0.10$	$0.39 \pm 0.10$
G293	$7.80 \pm 0.10$	$7.65 \pm 0.20$	$0.20 \pm 0.10$	$0.35 \pm 0.10$

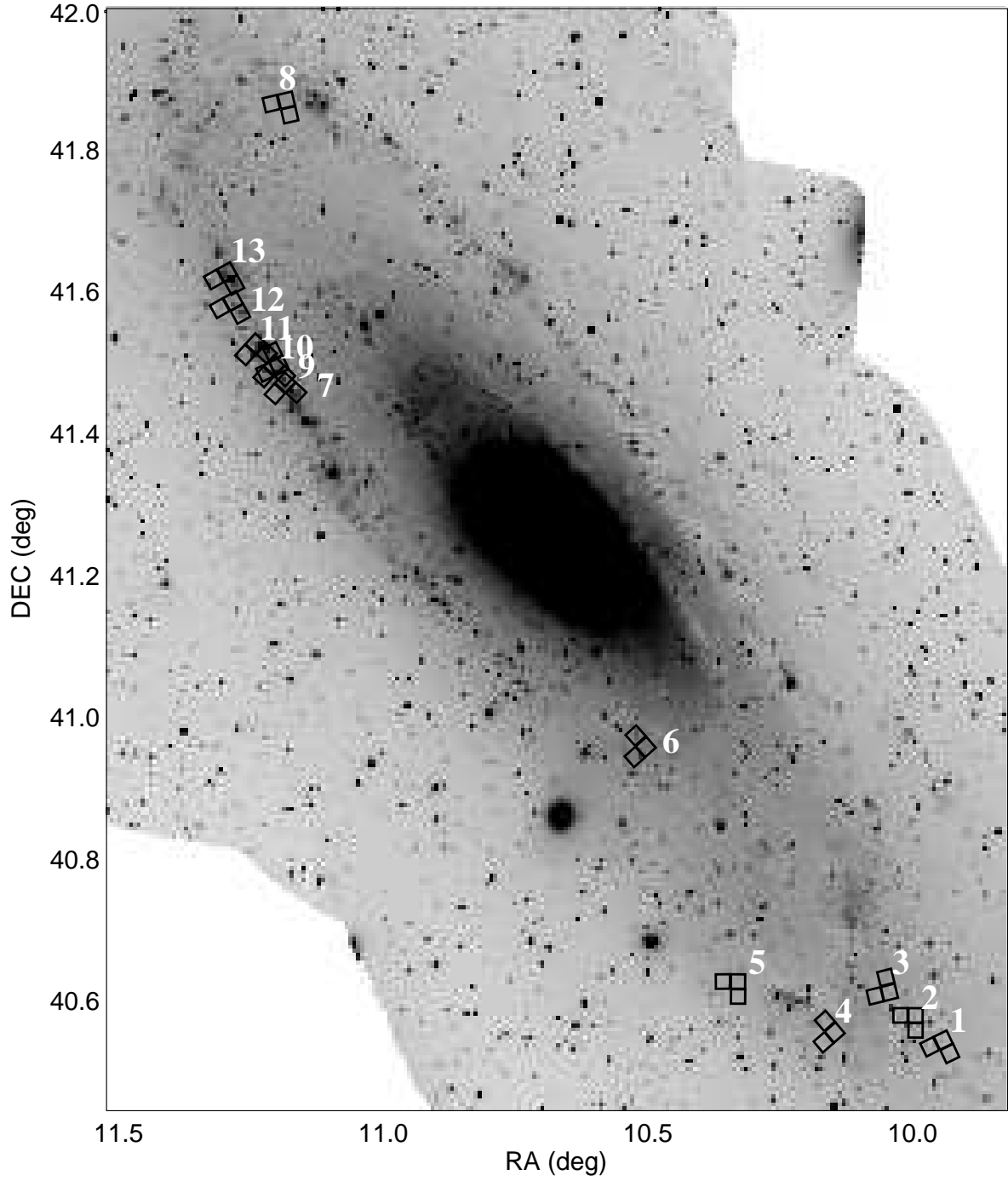


Fig. 1.— Positions of the HST fields taken from the HST archive. Shown are the fields that were observed through blue filters allowing detailed studies of the young main sequence population.



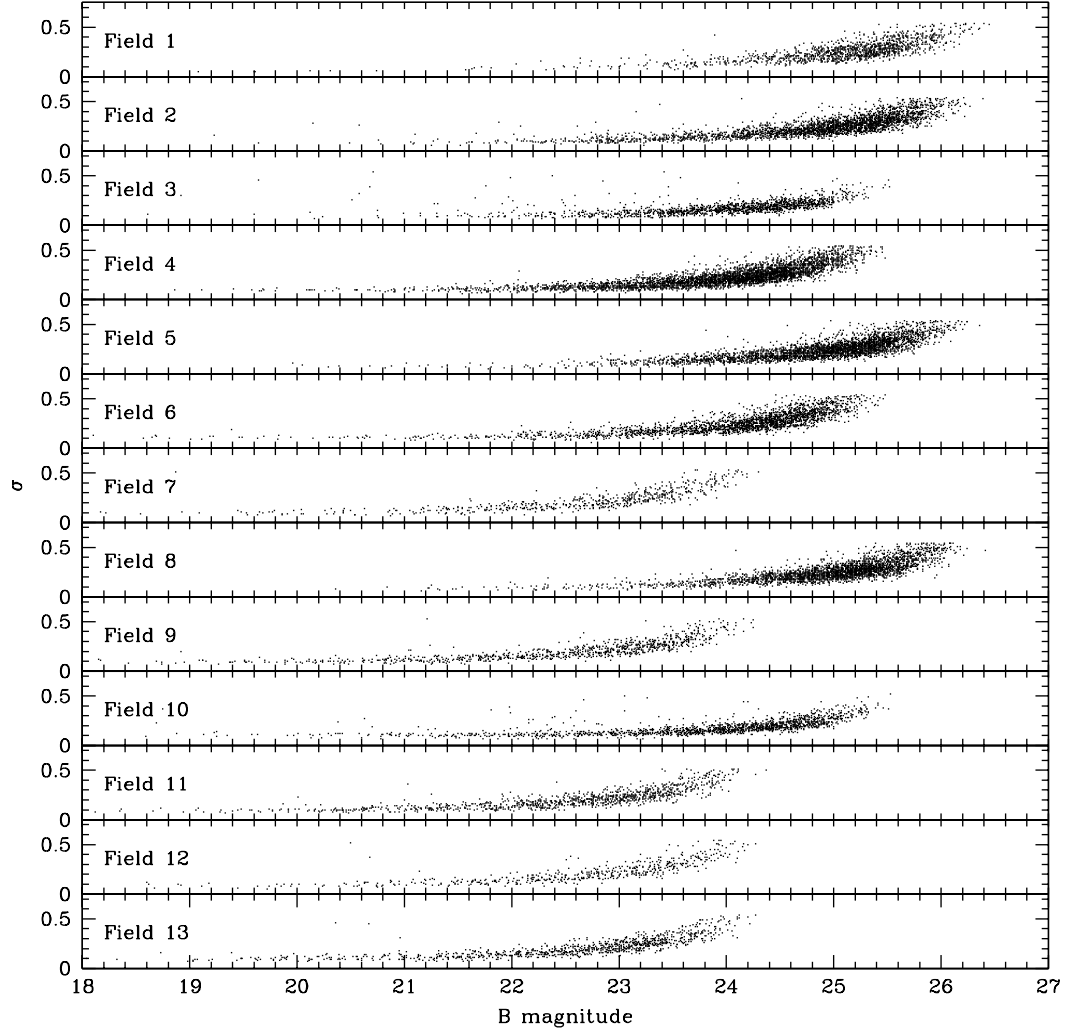


Fig. 2.— B band (F439W) photometric errors from ALLSTAR for the 13 fields.

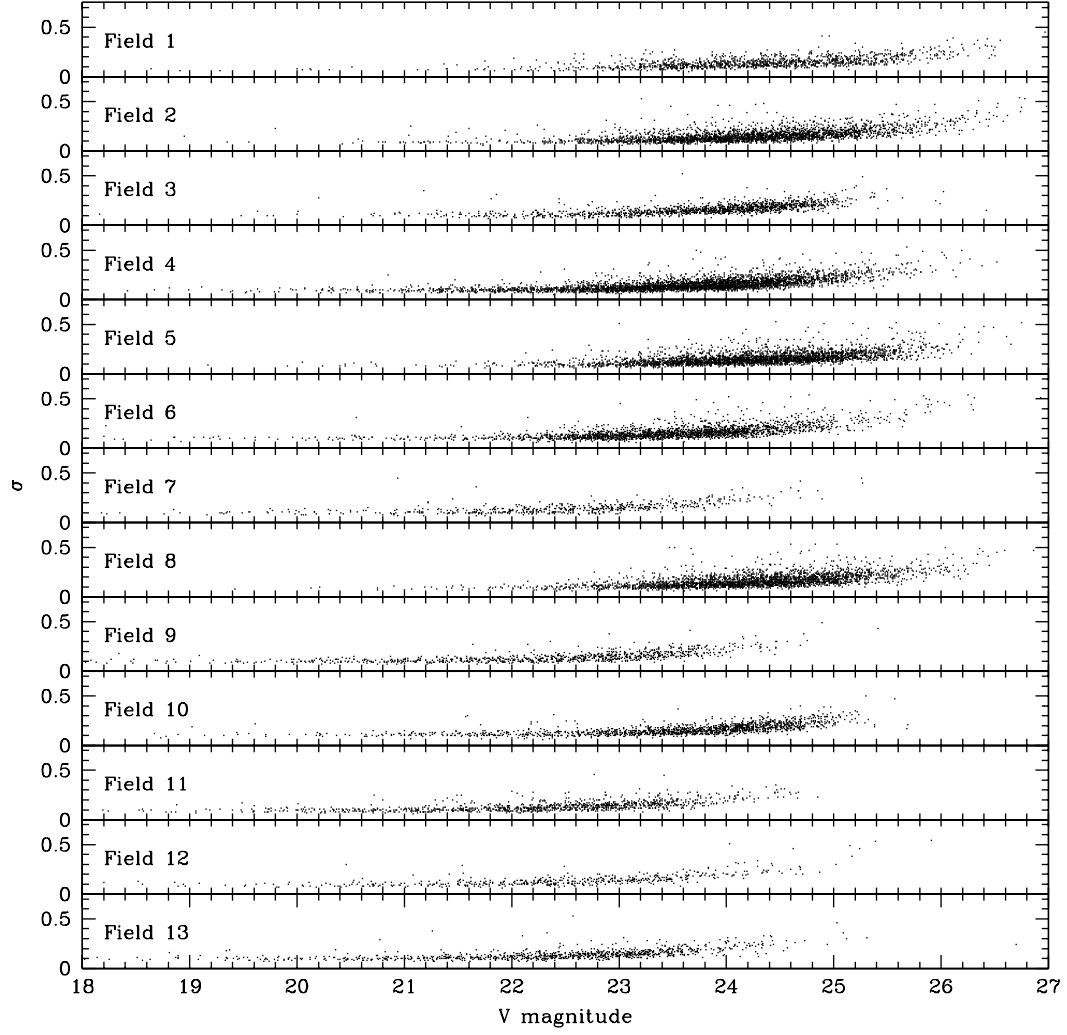


Fig. 3.— V band (F555W) photometric errors from ALLSTAR for the 13 fields.

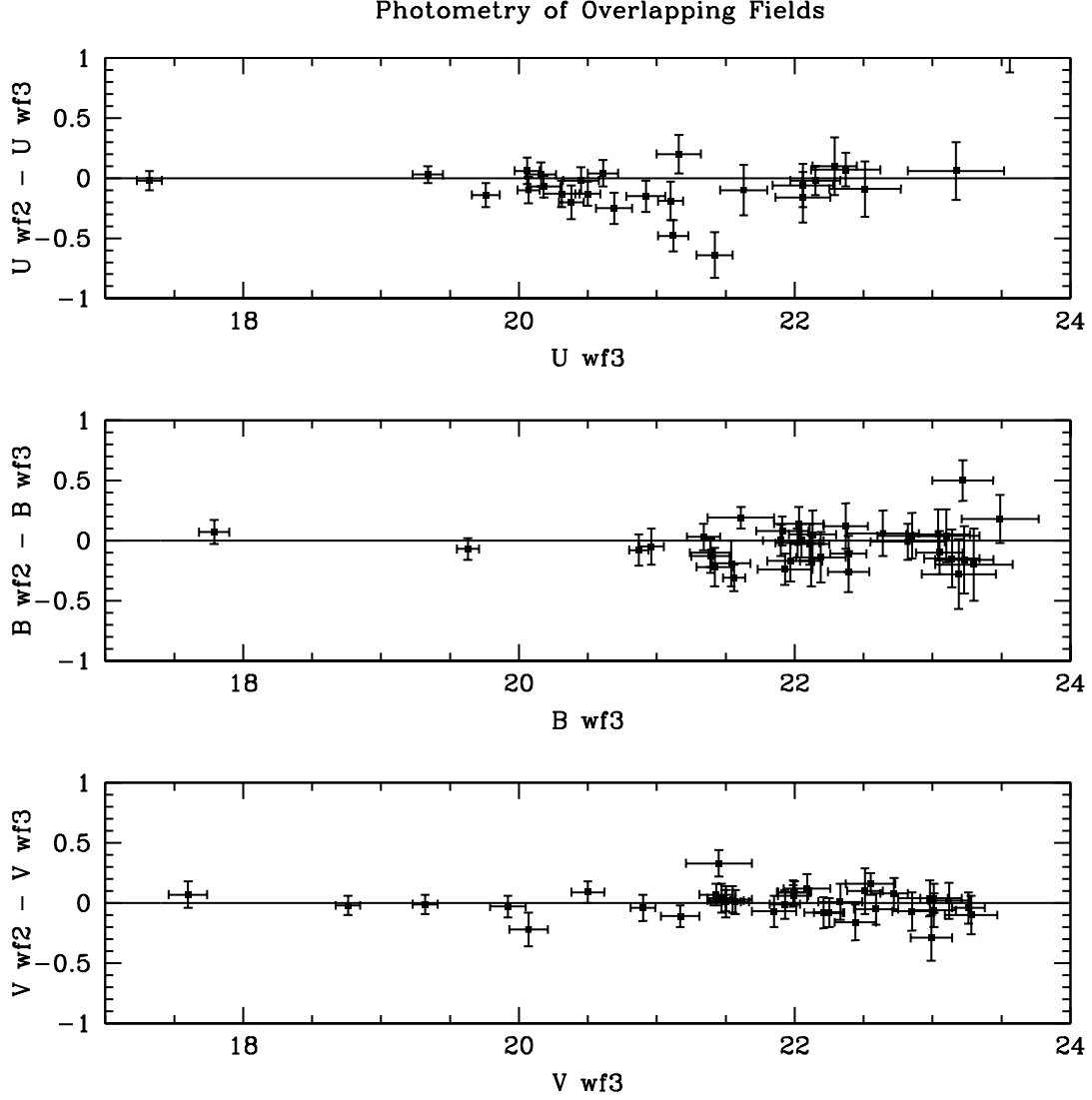


Fig. 4.— Residuals of photometry performed on the same stars in different fields in the F336W (U), F439W (B), and F555W (V), filters. The residuals of the independent measurements are consistent with zero. No systematic offset is seen.

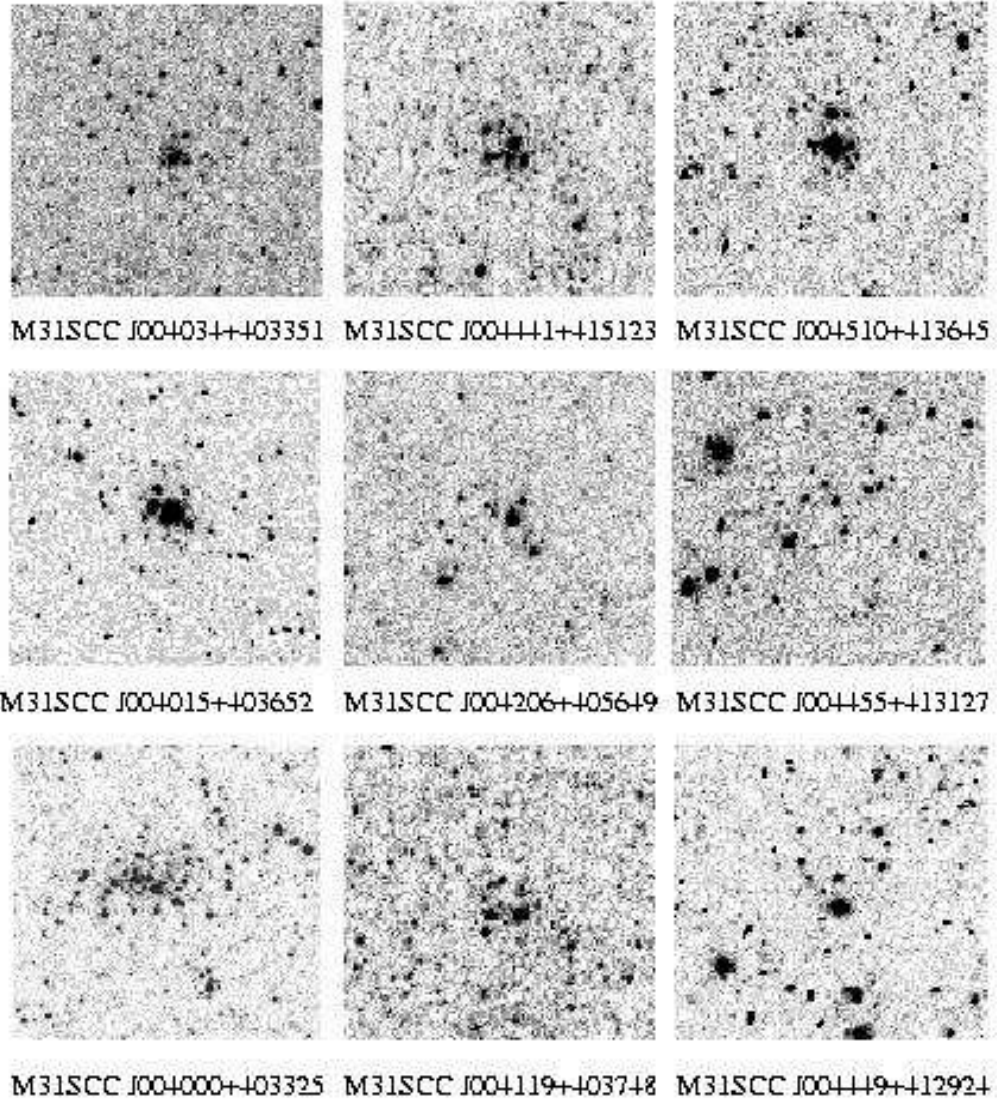


Fig. 5.— A random selection of 9 of our open cluster candidates. These B band (F439W) images are 12" by 12".

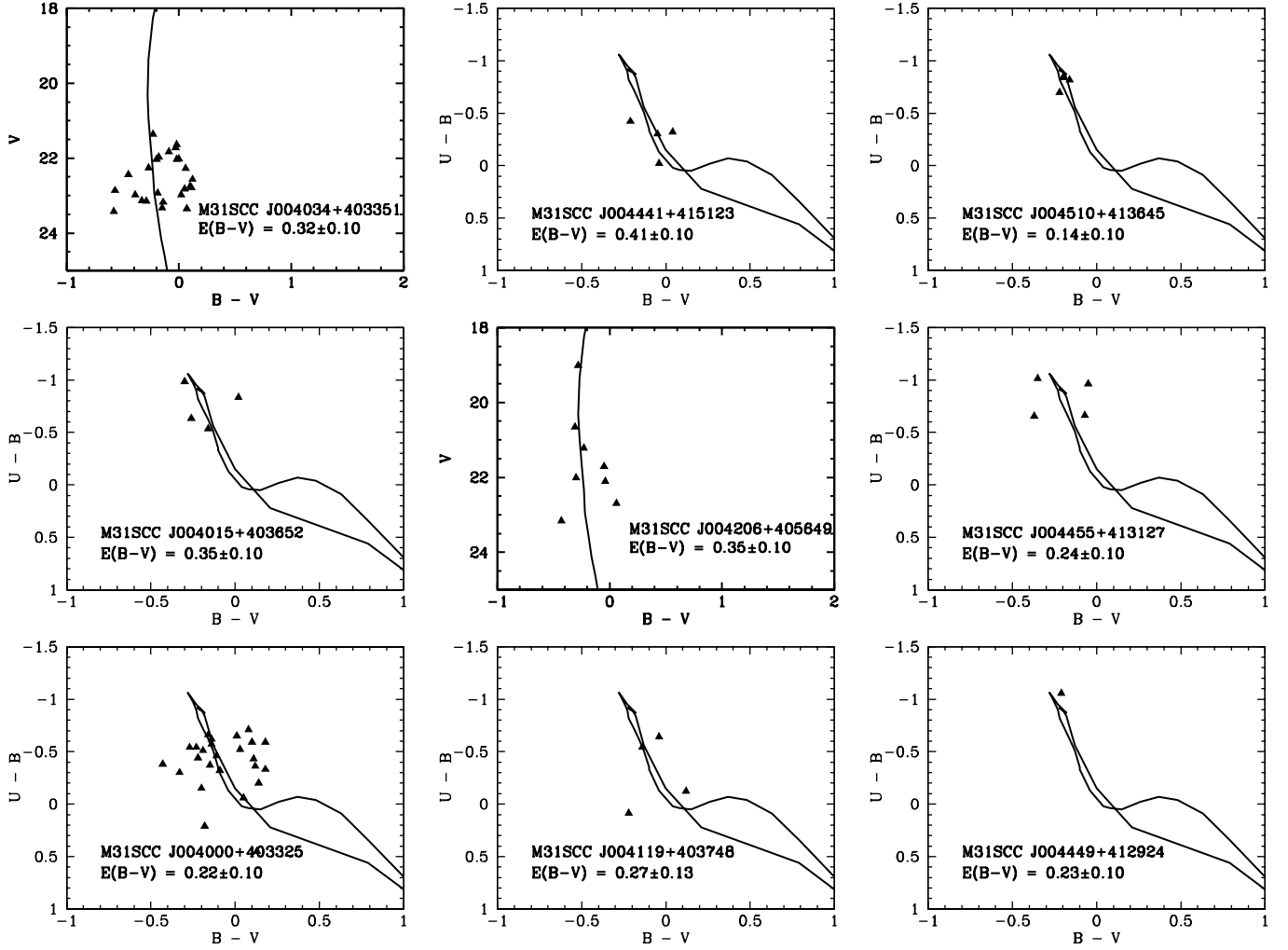


Fig. 6.— Reddening estimates of the 9 example clusters. The stellar colors and magnitudes have been corrected by the reddening values shown on the figures. These values gave the best fits to model upper main sequence colors. In cases where we did not have U band photometry, we relied on the B-V colors alone to determine reddening. Due to the sensitivity of WFPC2 in the U band, we occasionally were forced to make our first estimate of the reddening based on the colors of a single star detected in all three bands.

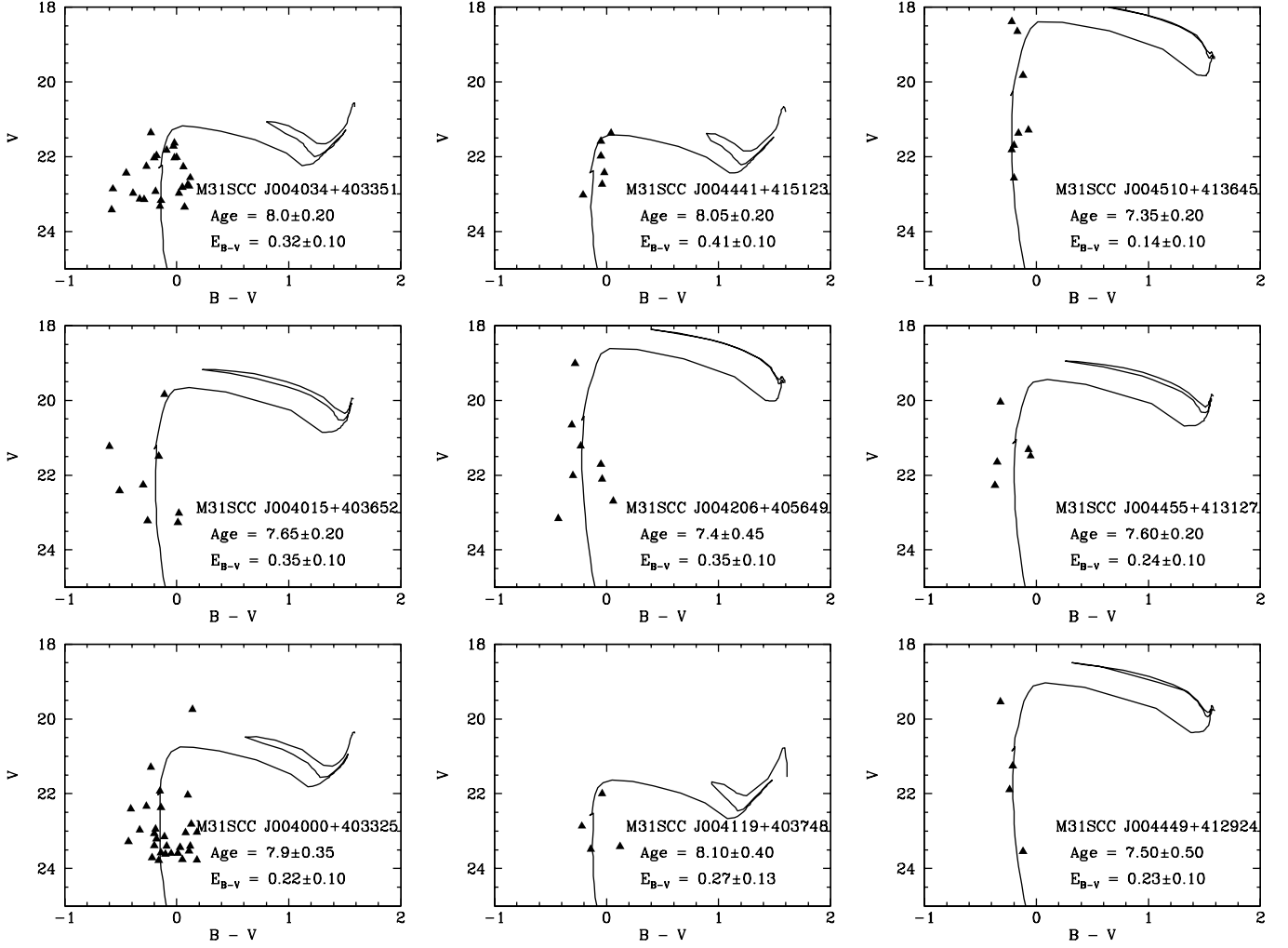


Fig. 7.— Age determinations of the 9 example clusters. The ages were determined by eye to fit the turnoff to the bright blue stars in the cluster. With so few stars, these ages estimates are very rough.

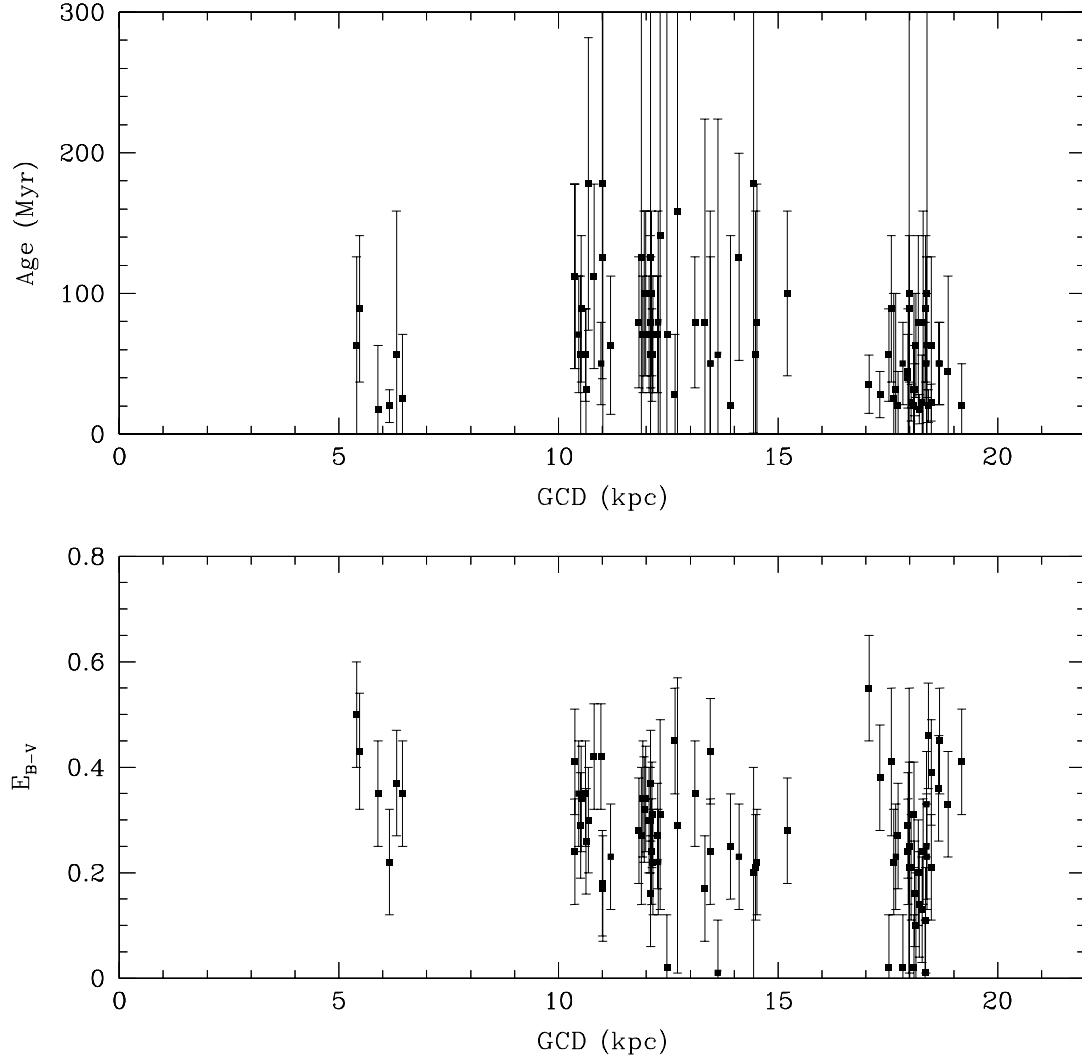


Fig. 8.— Plots of reddening and age vs. galactocentric distances for the cluster candidates. No patterns are seen with these rough estimates.

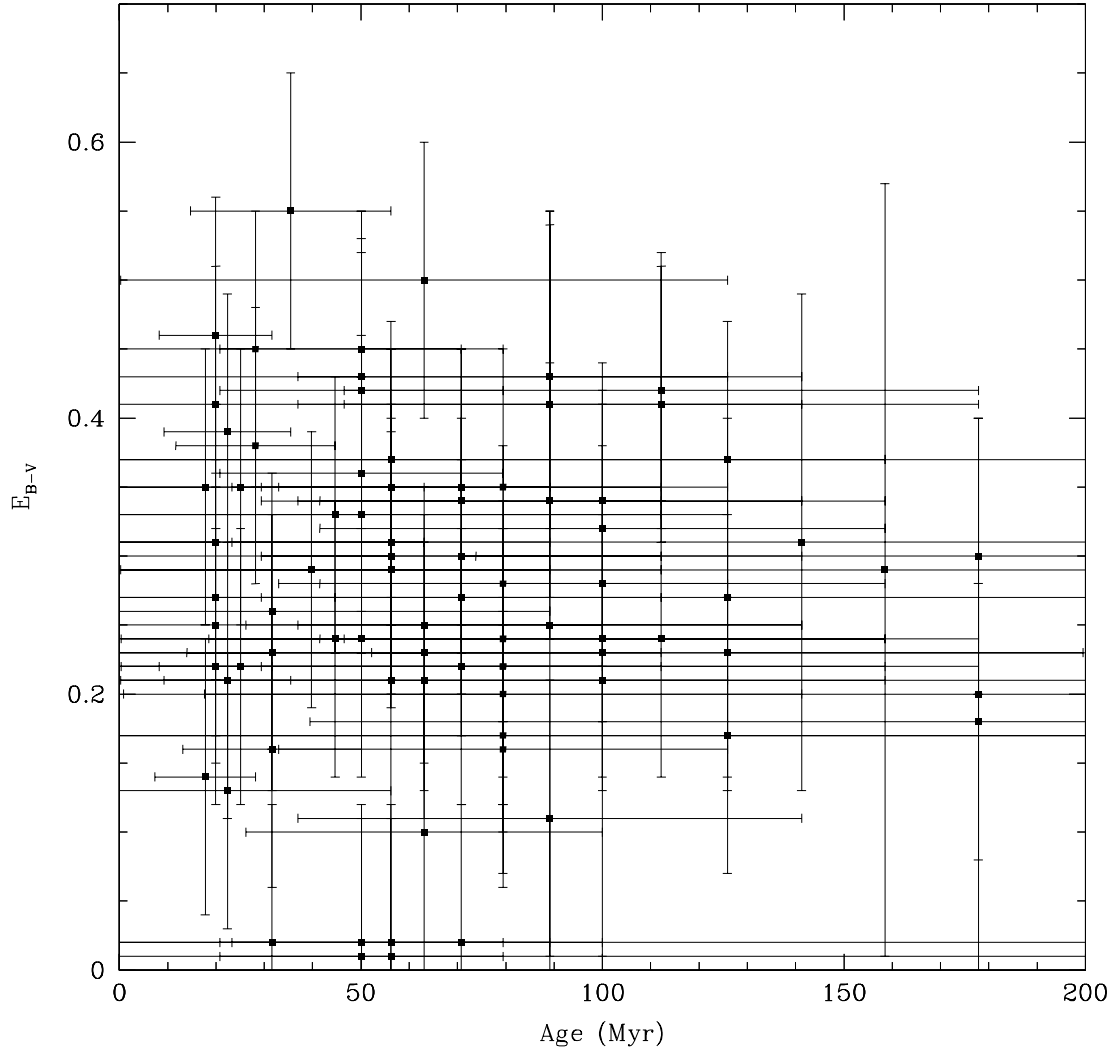


Fig. 9.— Reddening vs. age for the cluster candidates. Our algorithm was not sensitive to red clusters of stars so that there is a lack of high extinction, old clusters. The very low extinction clusters are likely to have field contaminants.